Rapid Communications

# Orientation dependent elastic stress concentration at tips of slender objects translating in viscoelastic fluids

Chuanbin Li
*Department of Mathematics, The Pennsylvania State University, University Park, Pennsylvania 16802, USA*

Becca Thomases and Robert D. Guy
*Department of Mathematics, University of California Davis, Davis, California 95616, USA*

(Received 7 September 2018; published 14 March 2019)

Elastic stress concentration at the tips of long slender objects moving in viscoelastic fluids has been observed in numerical simulations, but despite the prevalence of flagellated motion in complex fluids in many biological functions, the physics of stress accumulation near the tips has not been analyzed. Here, we theoretically investigate elastic stress development at the tips of slender objects by computing the leading-order viscoelastic correction to the equilibrium viscous flow around long cylinders, using the weak-coupling limit. In this limit, nonlinearities in the fluid are retained, allowing us to study the biologically relevant parameter regime of high Weissenberg number. We calculate a stretch rate from the viscous flow around cylinders to predict when large elastic stress develops at the tips, find thresholds for large stress development depending on orientation, and calculate greater stress accumulation near the tips of cylinders oriented parallel to the motion over perpendicular.

DOI: 10.1103/PhysRevFluids.4.031301

## I. INTRODUCTION

The interaction of slender objects such as cilia and flagella with surrounding viscoelastic fluid environments occurs in many important biological functions such as sperm swimming in mucus during fertilization and mucus clearance in the lungs. There has been much work devoted to understanding the effect of fluid elasticity in such systems including biological and physical experiments [1–4], asymptotic analysis for infinite-length swimmers [5–13], and numerical simulations of finite-length swimmers [14–19]. While flows around slender finite-length objects are essential to our understanding of the physics of micro-organism locomotion, our understanding of these flows in viscoelastic fluids is limited. Previous experimental and theoretical results have focused largely on the sedimentation of slender particles in the limit of vanishing relaxation time, i.e., the low Weissenberg number limit [20–26].

Numerical simulations of flagellated swimmers in viscoelastic fluids have shown the concentration of polymer elastic stress at the tips of slender objects [14,16,18,19] (see Fig. 1), but why the stress concentrates so strongly at the tips, and the effect of these stresses on micro-organism locomotion, is not understood. Unlike asymptotic theory [7–10,12,13], these simulations involve large-amplitude motions of finite-length objects, and these large elastic stresses that arise have a substantially different effect on the swimming motion than predicted by asymptotic analyses [18]. Experiments can measure kinematic changes [1,4], but not elastic stress, and thus the mechanisms of the observed behavioral responses cannot be explained by experiments alone.

It was observed in simulations [19] that the concentrated tip stresses are stronger for a cylinder moving parallel to its axis compared to a cylinder moving perpendicular to its axis. This orientation dependence of elastic stress at the tips is reversed from the orientation dependence of force on

 

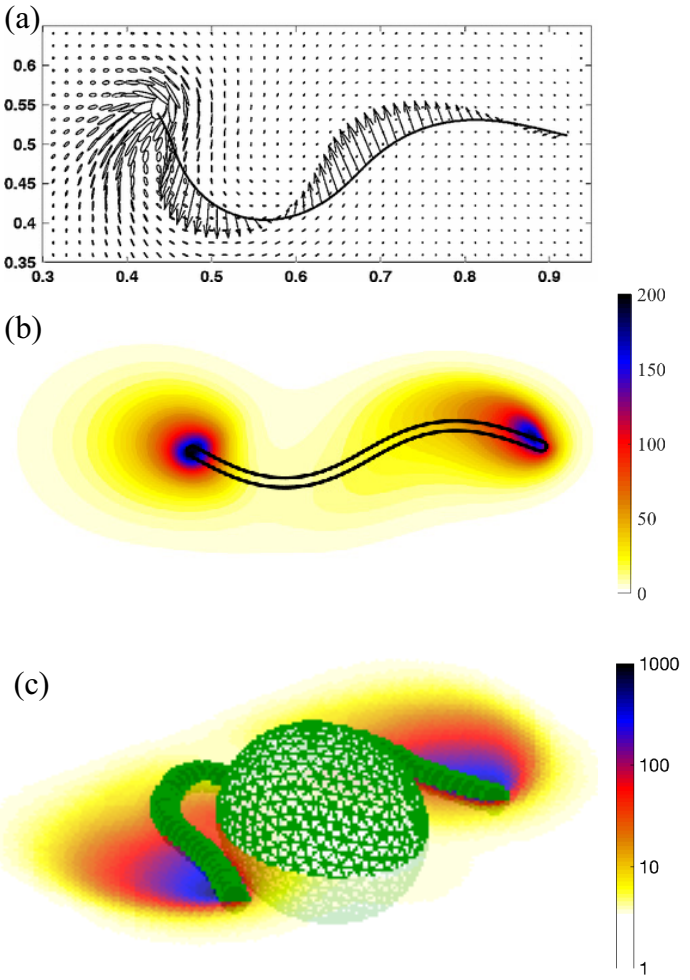


FIG. 1. (a) Two-dimensional (2D) flow around large-amplitude, finite-length undulatory swimmers; ellipses show the size and orientation of stress concentrated at the tail (reproduced from Ref. [14]). (b) 2D flow around a bending sheet; the color field shows strain energy density concentrated at the tips. (c) 3D flow around swimming biflagellated cells; the color field in the center plane shows strain energy density.

velocity in resistive force theory and related viscous fluid theories [27–32] which form the basis of much of our intuition about micro-organism locomotion without inertia. Classical viscous theories do not include tip effects, but previous results in viscoelastic fluids [14,16,18,19] suggest that the tip has a special role in the elastic stress development which has not been previously analyzed.

Previous work on the flow of viscoelastic fluids around slender objects has been done in the weakly nonlinear (or low Weissenberg number Wi) regime [20–26], but the large stress concentration at the tips of thin objects is a nonlinear effect and thus cannot be captured in a low Wi expansion. However, the highly nonlinear regime is challenging for numerical simulations [33], and this has limited the ability to probe the dynamics in this regime. As another approach, one can consider the limit of low polymer concentration, decoupling the stress and velocity. This method has been used to study stress localization for high Wi at extensional points and around objects [34–38].

The weak-coupling expansion, a formal asymptotic approximation in the limit of low polymer concentration, retains viscoelastic nonlinearities at leading order [39]. This method has been

successful in capturing high Wi effects for flow around a sphere in three dimensions (3D) [39], and in the study of the rheology of dilute suspensions in the low polymer concentration limit [40]. A similar stress localization in the wake of spheres has been observed experimentally [41,42], and theoretical predictions of shear thickening for strongly elastic dilute suspensions were in agreement with experimental observations [43].

Here, we use the weak-coupling expansion to study the equilibrium flow around, and resultant force on, cylinders translating either perpendicular, or parallel to the direction of motion, in a 3D viscoelastic fluid. Using this analysis, we explain the origin of the tip stresses, we predict a critical Weissenberg number for the flow transition based on viscous flow data, and we show how the tip stress accumulation depends on cylinder orientation.

## II. MODEL EQUATIONS

We examine the viscoelastic fluid flow around a stationary finite-length cylinder of radius $a$ with hemispherical caps driven by a fixed flow at infinity $\mathbf{U}_\infty$. We use the Oldroyd-B model of a viscoelastic fluid at zero Reynolds number, which is attractive as a frame-invariant, nonlinear, continuum model of a viscoelastic fluid that can capture the dominant effects of fluid elasticity, e.g., storage of the history of deformation on a characteristic timescale. The dimensionless system of equations is given by

$$\Delta\mathbf{u} - \nabla p + \beta\nabla\cdot\mathbf{C} = \mathbf{0}, \tag{1}$$

$$\nabla\cdot\mathbf{u} = \mathbf{0}, \tag{2}$$

$$\mathcal{D}_t[\mathbf{u}]\mathbf{C} = \mathrm{Wi}^{-1}\,\mathbf{I} + \left(\nabla\mathbf{u}\mathbf{C} + \mathbf{C}\nabla\mathbf{u}^T\right) - \mathrm{Wi}^{-1}\,\mathbf{C}, \tag{3}$$

for $\mathbf{u}$ the fluid velocity, $p$ the fluid pressure, and $\mathbf{C}$ the conformation tensor, a macroscopic average of the polymer orientation and stretching that is related to the polymer stress tensor by $\boldsymbol{\sigma}^p = \beta(\mathbf{C}-\mathbf{I})$. We use $\mathcal{D}_t[\mathbf{u}]$ to denote the material time derivative along the velocity field $\mathbf{u}$. The parameters $\beta$, the nondimensional polymer stiffness, and Wi, the Weissenberg number, or nondimensional relaxation time, are defined by

$$\beta = \frac{Gr}{\mu U}, \quad \mathrm{Wi} = \frac{\lambda U}{r}, \tag{4}$$

for $\mu$ the fluid viscosity, $\lambda$ the fluid relaxation time, $G$ the polymer elastic modulus, and $U = |\mathbf{U}_\infty|$.

The force on a stationary cylinder in a background flow is proportional to the rate at which energy is dissipated by the fluid. To calculate the dissipation rate we integrate the dot product of $(\mathbf{u}-\mathbf{U}_\infty)$ and Eq. (1) over the fluid domain $\Omega$ (exterior to the cylinder). After some manipulations and using the incompressibility constraint we obtain

$$\mathbf{U}_\infty\cdot\mathbf{F} = 2\int_\Omega D_{ij}D_{ij}\,dV + \beta\int_\Omega \frac{\partial u_i}{\partial x_j}C_{ij}\,dV, \tag{5}$$

where $D_{ij} = \frac{1}{2}(\frac{\partial u_i}{\partial x_j} + \frac{\partial u_j}{\partial x_i})$ is the rate of strain tensor, $\mathbf{F} = \int_{\partial\Omega}(\boldsymbol{\sigma}^n + \beta\mathbf{C})\cdot\mathbf{n}\,dS$ is the force on the cylinder, and $\boldsymbol{\sigma}^n = 2\mathbf{D} - p\mathbf{I}$ is the Newtonian stress tensor. Thus for a constant velocity at infinity, the force on the cylinder is proportional to the sum of the viscous dissipation rate and the rate at which energy is transferred to the polymers.

The polymer strain energy is $\mathcal{E} = \int_\Omega \mathrm{Tr}(\mathbf{C}-\mathbf{I})dV$ [44], and an equation for the strain energy is obtained by taking the trace of Eq. (3) and integrating over the fluid domain,

$$\frac{d}{dt}\mathcal{E} = 2\int_\Omega \frac{\partial u_i}{\partial x_j}C_{ij}\,dV - \mathrm{Wi}^{-1}\,\mathcal{E}. \tag{6}$$

Changes in the polymer energy come from the transfer of energy between the fluid and the polymer and energy lost to polymer relaxation. Therefore at steady state the rate of energy loss to the fluid is proportional to the polymer energy. By combining Eq. (5) with Eq. (6) one finds that at steady state the force on the cylinder is

$$\mathbf{U}_\infty \cdot \mathbf{F} = 2\int_\Omega D_{ij}D_{ij}\,dV + \frac{\beta}{2\,\mathrm{Wi}}\mathcal{E}. \tag{7}$$

Hence the strain energy $\mathcal{E}$ quantifies the force on the cylinder due to viscoelasticity.

## III. WEAK-COUPLING EXPANSION

Previous theoretical results on the polymeric contribution to a translating cylinder have used a second-order fluid expansion in the weakly nonlinear regime [26,45–48], where the nonlinearities associated with viscoelasticity are lost at leading order. We are interested in the regime of large-amplitude motions where large stress accumulates in the fluid, so we consider the *weakly coupled*, or small $\beta$, regime where the nonlinearities enter at leading order but the coupling between the polymer and fluid is higher order. The weak-coupling expansion was introduced for flow around a sphere in Ref. [39], and is similar to analyses of viscoelastic fluids using fixed velocity fields in the high Wi regime [49,50]. Analyses of viscoelastic fluids with fixed velocity fields have predicted transitions in behavior for high Wi at steady extensional points [34–38] and qualitatively similar transitions are also found in simulations where the velocity and the stress are fully coupled [38].

We expand the solutions in $\beta$, $\mathbf{u} \sim \mathbf{u}_0 + \beta\mathbf{u}_1$, $p \sim p_0 + \beta p_1$, and $\mathbf{C} \sim \mathbf{C}_0 + \beta\mathbf{C}_1$. At leading order, Eqs. (1) and (2) decouple from Eq. (3), and $\mathbf{u}_0$ is the solution for the viscous flow around the cylinder. The conformation tensor satisfies

$$\mathcal{D}_t[\mathbf{u}_0]\mathbf{C}_0 = \mathrm{Wi}^{-1}\,\mathbf{I} + \mathcal{S}[\mathbf{u}_0]\mathbf{C}_0 - \mathrm{Wi}^{-1}\,\mathbf{C}_0, \tag{8}$$

where $\mathcal{S}[\mathbf{u}_0]\mathbf{C}_0 \equiv (\nabla\mathbf{u}_0\mathbf{C}_0 + \mathbf{C}_0\nabla\mathbf{u}_0^T)$. On a given streamline, Eq. (8) is an ordinary differential equation (ODE) involving a source term, $\mathrm{Wi}^{-1}\,\mathbf{I}$, a stretching term, $\mathcal{S}[\mathbf{u}_0]$, and a relaxation term, $\mathrm{Wi}^{-1}\,\mathbf{C}_0$.

## IV. TIP STRESS DEVELOPMENT

We prescribe a unit flow in the $x$ direction, $\mathbf{U}_\infty = \mathbf{e}_x$, in the domain exterior to a cylinder that is oriented either parallel or perpendicular to the direction of flow, with no-slip boundary conditions on the cylinder walls. The circular cylinder has length $4\pi$, radius $a = 1$, and is capped at both ends with hemispheres. We solve the Stokes equations for $\mathbf{u}_0$ using a boundary integral method based on a regularized Green's function from the method of regularized Stokeslets [51–53]. We generate streamlines of the Newtonian flow $\mathbf{u}_0$ and evolve Eq. (8) along those streamlines. See Supplemental Material for more details [54].

In Fig. 2(a) we plot the Frobenius norm (defined $\|\mathbf{A}\| \equiv \sqrt{A_{ij}A_{ij}}$) of the leading-order viscous stress tensor $2\mathbf{D}_0$ in the center plane for cylinders oriented (i) parallel and (ii) perpendicular to the flow. Note that the viscous stress near the middle of the cylinders is two or three times smaller than that at the tips. In Fig. 2(b) we show color fields of the leading-order polymer strain energy density $\mathrm{Tr}(\mathbf{C}_0 - \mathbf{I})$, for two different Weissenberg numbers (i), (ii) $\mathrm{Wi} = 1$ and (iii), (iv) $\mathrm{Wi} = 5$. For $\mathrm{Wi} = 1$ the elastic stress is concentrated at the tips as the viscous stress, and on the same scale as the viscous stress. For $\mathrm{Wi} = 5$, however, the elastic stress at the tips is more than 100 times larger than for $\mathrm{Wi} = 1$, and concentrated in the wake. This nonlinear response has been seen before in analyses of flow around a circle in 2D [55–57] and around a sphere in 3D [39]. However, in Figs. 2(b)(iii) and 2(b)(iv) we also see that the stress in the wake of the cylinder that is oriented parallel to the direction of the flow is about ten times larger than that for the cylinder oriented perpendicular to the direction of flow. We examine the Newtonian flow that drives the stress growth to understand what sets the transition in Wi, and how the cylinder orientation impacts stress growth so dramatically for large Wi.

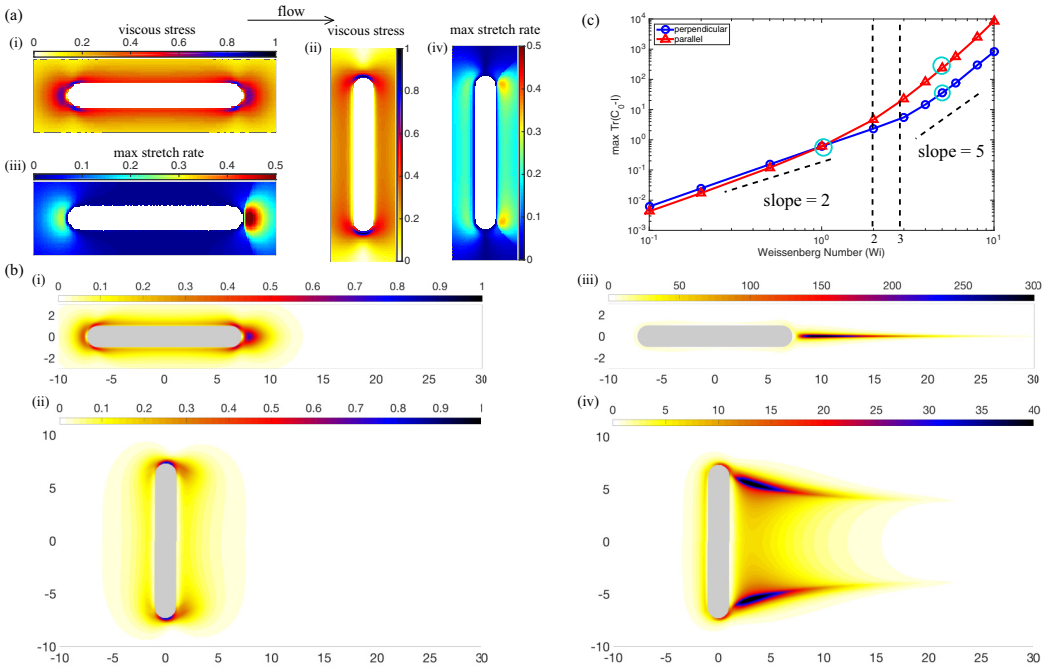


FIG. 2. (a) Norm of viscous stress in the center plane for cylinders oriented (i) parallel (max $\|2\mathbf{D}_0^{\parallel}\| \approx 0.78$) and (ii) perpendicular (max $\|2\mathbf{D}_0^{\perp}\| \approx 0.95$) to flow; stretch rates of viscous flow for cylinders oriented (iii) parallel (max $\nu^{\parallel} \approx 0.5$) and (iv) perpendicular (max $\nu^{\perp} \approx 0.34$) to flow. Flow goes from left to right. (b) $\mathrm{Tr}(\mathbf{C}_0 - \mathbf{I})$ in the center plane for cylinders with (i), (ii) $\mathrm{Wi} = 1$ and (iii), (iv) $\mathrm{Wi} = 5$ (note the difference in scale). (c) Maximum of $\mathrm{Tr}(\mathbf{C}_0 - \mathbf{I})$ as a function of Wi for the two orientations, in log scales. Dotted lines show the two critical Weissenberg numbers $\mathrm{Wi} \approx 2$ and $\mathrm{Wi} \approx 3$, and cyan circles indicate Wi values pictured in (b).

At a fixed point in the flow, the real parts of the eigenvalues of the operator $\mathcal{S}[\mathbf{u}_0]$, defined in Eq. (8), set the growth (or decay) rates of $\mathbf{C}_0$ due to stretching (or compression). The solution to the eigenvalue problem $\mathcal{S}[\mathbf{u}]\mathbf{C} = \nu\mathbf{C}$ is $\mathbf{C} = \mathbf{v}_i\mathbf{v}_j^T$, $\nu_{ij} = \mu_i + \mu_j$, where $\mu_i$ is an eigenvalue of $\nabla\mathbf{u}$ with corresponding eigenvector $\mathbf{v}_i$. We define the maximum stretch rate $\nu$ at a point as

$$\nu = 2\max\{\mathrm{Re}[\Lambda(\nabla\mathbf{u}_0)]\}, \tag{9}$$

where $\Lambda(A)$ is the set of eigenvalues of the matrix $A$. In regions of the flow where $\nu - \mathrm{Wi}^{-1} > 0$, or $\nu\,\mathrm{Wi} > 1$, stretching outpaces relaxation, and while fluid particles remain in these stretching regions they experience unbounded stress growth.

In Fig. 2(a) we plot $\nu$ in the center plane for the cylinder oriented parallel (iii) and the cylinder oriented perpendicular (iv). The maximum stretch rate for both cylinders occurs in the wake of the cylinder, i.e., the maximum stretch rate contains information about flow directionality that is missing from Figs. 2(a)(i) and 2(a)(ii). We see that the cylinder oriented parallel to motion has $\max(\nu^{\parallel}) \approx 0.5$, thus $\mathrm{Wi}^{\parallel} \approx 2$ is a threshold for stretching outpacing relaxation in regions of this flow. The maximum for the perpendicularly oriented cylinder is smaller, $\max(\nu^{\perp}) \approx 0.34$, corresponding to a threshold $\mathrm{Wi}^{\perp} \approx 3$ for large stress growth. For the perpendicularly oriented cylinder, the flow in the regions of high viscous stress near the tip is locally a shear flow, whereas the local flow is extensional (which is known to lead to more rapid elastic stress growth [58]) near the tips of the cylinder oriented parallel. The difference in flow type is reflected in the maximum stretch rate which is largest near the trailing tip of the cylinder oriented parallel to the motion where the viscous stress

is largest. For the perpendicularly oriented cylinder, the strongest extension is behind the cylinder where the viscous stresses are weaker.

In Fig. 2(c) we plot max $\mathrm{Tr}(\mathbf{C}_0 - \mathbf{I})$ for $\mathrm{Wi} \leqslant 10$. For both orientations, the maximum of $\mathrm{Tr}(\mathbf{C}_0 - \mathbf{I})$ scales as $\mathrm{Wi}^2$ below $\mathrm{Wi} \approx 2$, and scales as $\mathrm{Wi}^5$ above $\mathrm{Wi} \approx 3$. The cylinder oriented parallel to the motion has a larger maximum stretch rate and thus it enters the regime of large stress growth for lower Wi than the perpendicularly oriented cylinder, leading to larger stress for a fixed Wi beyond the threshold $\mathrm{Wi}^{\parallel} \approx 2$. Recall that the contribution to the force from the polymeric stress scales as $\frac{\beta}{2\mathrm{Wi}}\mathcal{E}$ and thus for low Wi there is an $O(\mathrm{Wi})$ contribution to the force whereas for high Wi the contribution is $O(\mathrm{Wi}^4)$. Theoretical results have predicted similar scalings for related problems [39,49,50].

## V. VISCOELASTIC CORRECTION TO FORCE

We expand the force on a cylinder to first order in $\beta$ as

$$\mathbf{F} \sim \int_{\partial\Omega} \boldsymbol{\sigma}_0^n \cdot \mathbf{n} + \beta\left(\boldsymbol{\sigma}_1^n + \mathbf{C}_0\right) \cdot \mathbf{n}\, dS \equiv \mathbf{F}_0 + \beta\mathbf{F}_1. \tag{10}$$

We avoid computing $\mathbf{u}_1$, the first-order correction to the velocity, by using reciprocal relations [26,45–48], as has been done before in many calculations of non-Newtonian corrections at low Reynolds number. In addition, because the flow and force are parallel for these orientations, we obtain the magnitude of $\mathbf{F}_1$ as

$$F_1 = \mathrm{Wi}^{-1} \int_{\Omega} \mathrm{Tr}(\mathbf{C}_0 - \mathbf{I}) dV. \tag{11}$$

Details of our calculation are provided in Supplemental Material [54]. Thus the viscoelastic correction to the force is proportional to the integral of the trace of the leading-order polymer stress tensor over the fluid domain.

In Fig. 3(a) we plot the viscoelastic force correction $F_1$ normalized by $F_0^{\perp} = 65$ (note $F_0^{\parallel} = 48$) for $\mathrm{Wi} \leqslant 10$ for each cylinder orientation. We see that in the expansion the $O(\beta)$ force correction is up to 25 times the viscous force for large Wi. The perpendicular force correction is larger than the parallel force correction, however, Fig. 3(b) shows $F_1^{\parallel}/F_1^{\perp}$ (left-hand axes), and beyond $\mathrm{Wi} \approx 2$ (the parallel stress growth threshold), $F_1^{\parallel}$ increases more than $F_1^{\perp}$, and this continues until about $\mathrm{Wi} \approx 6$ where the ratio starts to decrease again. Since we are interested in the "tip effect," we calculate the contribution to the force from a single tip.

We define this tip force by restricting the integration domain in Eq. (11) to a subdomain exterior to the cylinder that contains only one tip. In Fig. 3(d) we show the tip of the perpendicular cylinder with the strain energy density for $\mathrm{Wi} = 5$. We consider a streamline that approaches very close to the tip in the center plane and we evolve the streamline until it levels off for large $x$, and we define the value it approaches, $y_{\mathrm{tip}} = 3.41$, as shown in Fig. 3(d). With this we define

$$F_1^{\mathrm{tip}} = \mathrm{Wi}^{-1} \int_{\Omega\setminus\{y<y_{\mathrm{tip}}\}} \mathrm{Tr}(\mathbf{C}_0 - \mathbf{I}) dV. \tag{12}$$

In Fig. 3(c) we plot $F_1^{\mathrm{tip}}/F_0^{\perp}$ for $\mathrm{Wi} \leqslant 10$ for each cylinder orientation, and the ratio of tip force corrections in Fig. 3(b) (right-hand axes). Beyond the threshold $\mathrm{Wi}^{\parallel} \approx 2$, the parallel force correction at the tip is larger than the perpendicular force correction, and the parallel force correction is double the perpendicular force correction from the tip at high Wi.

## VI. DISCUSSION

Using the viscous flow field around cylinders we predict a critical Wi beyond which a large stress "tip effect" occurs, and we find that the critical Wi is orientation dependent. There are larger

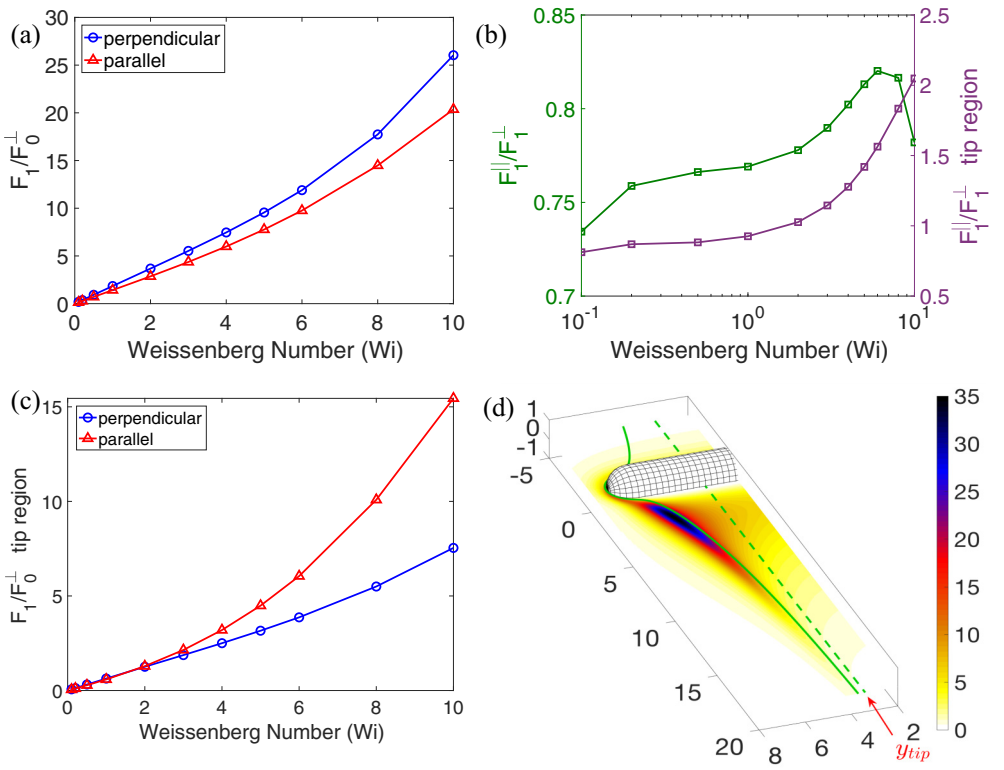


FIG. 3. (a) $F_1/F_0^\perp$ (perpendicular and parallel), (b) parallel to perpendicular ratio of $F_1$: Whole domain (left axes), tip region (right axes). (c) $F_1$ restricted to the tip (perpendicular and parallel). (d) Diagram illustrating the definition of $y_{\text{tip}}$.

elastic stresses in the wake of cylinders oriented parallel to the direction of motion compared to cylinders oriented perpendicular to the flow. The flow type (shear or extensional) is orientation dependent and is reflected in the larger maximum stretch rate for the cylinder oriented parallel. The maximum stretch rate is defined from the eigenvalues of the operator $\mathcal{S}$ in Eq. (8), and this operator appears in all differential models of viscoelasticity, including models which incorporate additional non-Newtonian effects such as shear thinning. Hence we conjecture that the transitions we have identified are not specific to the Oldroyd-B model, although the quantitative values of stress accumulation beyond the transitions will depend on the model.

We explored other tip shapes and found that varying curvature at the tip did not effect the qualitative results; the maximum stretch rate was always largest near the tip, and greater for cylinders oriented parallel to the motion. The analysis given used the rod thickness to define the characteristic length scale and hence thinner rods will exhibit large stress growth at a lower relaxation time. Although the tip effect is independent of the length, the relative contribution to the total force from the tip depends on the length, and hence quantifying the role of the tip effect on locomotion requires more investigation. Nevertheless, based on past numerical simulations of flagellated swimmers, it is clear that this tip effect is significant.

In Ref. [19] we observed elastic stress accumulation at flagellar tips in a simulation of a bi-flagellated alga cell swimming using experimentally measured kinematics. The stress accumulation was greater on the return stroke when the flagellar tips were oriented parallel to the direction of motion than when oriented perpendicular to the motion. The steady-state analysis of the tip effect

presented here helps explain the physics behind these observations made in Ref. [19], but generally details of the stroke kinematics, including time dependence, will effect how stresses develop around flagellated swimmers. We are able to make predictions about critical Weissenberg numbers for steady flows by looking at the maximum stretch rates, but this tool could be useful for other gaits and even in experimental settings where flow fields are obtainable but the location and concentration of stress are not measurable.

## ACKNOWLEDGMENTS

The authors thank David Stein for interesting discussions and suggestions on this work. R.D.G. and B.T. were supported in part by NSF Grant No. DMS-1664679.

[1] X. N. Shen and P. E. Arratia, Undulatory Swimming in Viscoelastic Fluids, Phys. Rev. Lett. **106**, 208101 (2011).
[2] B. Liu, T. R Powers, and K. S. Breuer, Force-free swimming of a model helical flagellum in viscoelastic fluids, Proc. Natl. Acad. Sci. USA **108**, 19516 (2011).
[3] J. Espinosa-Garcia, E. Lauga, and R. Zenit, Fluid elasticity increases the locomotion of flexible swimmers, Phys. Fluids **25**, 031701 (2013).
[4] B. Qin, A. Gopinath, J. Yang, J. P. Gollub, and P. E. Arratia, Flagellar kinematics and swimming of algal cells in viscoelastic fluids, Sci. Rep. **5**, 9190 (2015).
[5] T. K. Chaudhury, On swimming in a visco-elastic liquid, J. Fluid Mech. **95**, 189 (1979).
[6] G. R. Fulford, D. F. Katz, and R. L. Powell, Swimming of spermatozoa in a linear viscoelastic fluid, Biorheology **35**, 295 (1998).
[7] H. C. Fu, T. R. Powers, and C. W. Wolgemuth, Theory of Swimming Filaments in Viscoelastic Media, Phys. Rev. Lett. **99**, 258101 (2007).
[8] H. C. Fu, C. W. Wolgemuth, and T. R. Powers, Beating patterns of filaments in viscoelastic fluids, Phys. Rev. E **78**, 041913 (2008).
[9] E. Lauga, Propulsion in a viscoelastic fluid, Phys. Fluids **19**, 83104 (2007).
[10] H. C. Fu, C. W. Wolgemuth, and T. R. Powers, Swimming speeds of filaments in nonlinearly viscoelastic fluids, Phys. Fluids **21**, 033102 (2009).
[11] M. Dasgupta, B. Liu, H. C. Fu, M. Berhanu, K. S. Breuer, T. R. Powers, and A. Kudrolli, Speed of a swimming sheet in Newtonian and viscoelastic fluids, Phys. Rev. E **87**, 013015 (2013).
[12] E. E. Riley and E. Lauga, Enhanced active swimming in viscoelastic fluids, Europhys. Lett. **108**, 34003 (2014).
[13] G. J. Elfring and G. Goyal, The effect of gait on swimming in viscoelastic fluids, J. Non-Newtonian Fluid Mech. **234**, 8 (2016).
[14] J. Teran, L. Fauci, and M. Shelley, Viscoelastic Fluid Response Can Increase the Speed and Efficiency of a Free Swimmer, Phys. Rev. Lett. **104**, 038101 (2010).
[15] S. E. Spagnolie, B. Liu, and T. R. Powers, Locomotion of Helical Bodies in Viscoelastic Fluids: Enhanced Swimming at Large Helical Amplitudes, Phys. Rev. Lett. **111**, 068101 (2013).
[16] B. Thomases and R. D. Guy, Mechanisms of Elastic Enhancement and Hindrance for Finite-Length Undulatory Swimmers in Viscoelastic Fluids, Phys. Rev. Lett. **113**, 098102 (2014).
[17] D. Salazar, A. M. Roma, and H. D. Ceniceros, Numerical study of an inextensible, finite swimmer in Stokesian viscoelastic flow, Phys. Fluids **28**, 063101 (2016).
[18] B. Thomases and R. D. Guy, The role of body flexibility in stroke enhancements for finite-length undulatory swimmers in viscoelastic fluids, J. Fluid Mech. **825**, 109 (2017).
[19] C. Li, B. Qin, A. Gopinath, P. E. Arratia, B. Thomases, and R. D. Guy, Flagellar swimming in viscoelastic fluids: role of fluid elastic stress revealed by simulations based on experimental data, J. R. Soc. Interface **14**, 20170289 (2017).

[20] L. G. Leal, The slow motion of slender rod-like particles in a second-order fluid, J. Fluid Mech. **69**, 305 (1975).
[21] S. Kim, The motion of ellipsoids in a second order fluid, J. Non-Newtonian Fluid Mech. **21**, 255 (1986).
[22] K. Chiba, K.-W. Song, and A. Horikawa, Motion of a slender body in quiescent polymer solutions, Rheol. Acta **25**, 380 (1986).
[23] D. D. Joseph, Flow induced microstructure in Newtonian and viscoelastic fluids, University of Minnesota Supercomputing Institute Research Report No. UMSI 99/97, 1999 (unpublished).
[24] P. Y. Huang, H. H. Hu, and D. D. Joseph, Direct simulation of the sedimentation of elliptic particles in Oldroyd-B fluids, J. Fluid Mech. **362**, 297 (1998).
[25] G. P. Galdi, Slow steady fall of rigid bodies in a second-order fluid, J. Non-Newtonian Fluid Mech. **90**, 81 (2000).
[26] V. Dabade, N. K. Marath, and G. Subramanian, Effects of inertia and viscoelasticity on sedimenting anisotropic particles, J. Fluid Mech. **778**, 133 (2015).
[27] G. J. Hancock, The self-propulsion of microscopic organisms through liquids, Proc. R. Soc. London, Ser. A **217**, 96 (1953).
[28] J. Gray and G. J. Hancock, The propulsion of sea-urchin spermatozoa, J. Exp. Biol. **32**, 802 (1955).
[29] J. B. Keller and S. I. Rubinow, Slender-body theory for slow viscous flow, J. Fluid Mech. **75**, 705 (1976).
[30] J. Lighthill, Flagellar hydrodynamics, SIAM Rev. **18**, 161 (1976).
[31] R. E. Johnson and C. J. Brokaw, Flagellar hydrodynamics. A comparison between resistive-force theory and slender-body theory, Biophys. J. **25**, 113 (1979).
[32] R. E. Johnson, An improved slender-body theory for Stokes flow, J. Fluid Mech. **99**, 411 (1980).
[33] R. G. Owens and T. N. Phillips, *Computational Rheology* (World Scientific, Singapore, 2002).
[34] J. M. Rallison and E. J. Hinch, Do we understand the physics in the constitutive equation? J. Non-Newtonian Fluid Mech. **29**, 37 (1988).
[35] O. G. Harlen, High-Deborah-number flow of a dilute polymer solution past a sphere falling along the axis of a cylindrical tube, J. Non-Newtonian Fluid Mech. **37**, 157 (1990).
[36] O. G. Harlen, J. M. Rallison, and M. D. Chilcott, High-Deborah-number flows of dilute polymer solutions, J. Non-Newtonian Fluid Mech. **34**, 319 (1990).
[37] M. Renardy, A comment on smoothness of viscoelastic stresses, J. Non-Newtonian Fluid Mech. **138**, 204 (2006).
[38] B. Thomases and M. Shelley, Emergence of singular structures in Oldroyd-B fluids, Phys. Fluids **19**, 103103 (2007).
[39] M. N. J. Moore and M. J. Shelley, A weak-coupling expansion for viscoelastic fluids applied to dynamic settling of a body, J. Non-Newtonian Fluid Mech. **183**, 25 (2012).
[40] D. L. Koch, E. F. Lee, and I. Mustafa, Stress in a dilute suspension of spheres in a dilute polymer solution subject to simple shear flow at finite Deborah numbers, Phys. Rev. Fluids **1**, 013301 (2016).
[41] A. Acharya, R. A. Mashelkar, and J. Ulbrecht, Flow of inelastic and viscoelastic fluids past a sphere, Rheol. Acta **15**, 454 (1976).
[42] M. T. Arigo and G. H. McKinley, An experimental investigation of negative wakes behind spheres settling in a shear-thinning viscoelastic fluid, Rheol. Acta **37**, 307 (1998).
[43] R. Scirocco, J. Vermant, and J. Mewis, Shear thickening in filled Boger fluids, J. Rheol. **49**, 551 (2005).
[44] R. B. Bird, R. C. Armstrong, O. Hassager, and C. F. Curtiss, *Dynamics of Polymeric Liquids* (Wiley, New York, 1977), Vol. 1.
[45] L. G. Leal, The motion of small particles in non-Newtonian fluids, J. Non-Newtonian Fluid Mech. **5**, 33 (1979).
[46] J. Happel and H. Brenner, *Low Reynolds Number Hydrodynamics: With Special Applications to Particulate Media* (Springer, Berlin, 2012), Vol. 1.
[47] H. A Stone and A. D. T. Samuel, Propulsion of Microorganisms by Surface Distortions, Phys. Rev. Lett. **77**, 4102 (1996).
[48] G. J. Elfring, A note on the reciprocal theorem for the swimming of simple bodies, Phys. Fluids **27**, 023101 (2015).

[49] M. Renardy, Asymptotic structure of the stress field in flow past a cylinder at high Weissenberg number, J. Non-Newtonian Fluid Mech. **90**, 13 (2000).
[50] P. Wapperom and M. Renardy, Numerical prediction of the boundary layers in the flow around a cylinder using a fixed velocity field, J. Non-Newtonian Fluid Mech. **125**, 35 (2005).
[51] R. Cortez, The method of regularized Stokeslets, SIAM J. Sci. Comput. **23**, 1204 (2001).
[52] R. Cortez, L. Fauci, and A. Medovikov, The method of regularized Stokeslets in three dimensions: Analysis, validation, and application to helical swimming, Phys. Fluids **17**, 031504 (2005).
[53] C. Pozrikidis, *Boundary Integral and Singularity Methods for Linearized Viscous Flow* (Cambridge University Press, Cambridge, UK, 1992).
[54] See Supplemental Material at http://link.aps.org/supplemental/10.1103/PhysRevFluids.4.031301 for details of the numerical method and validation, as well as a derivation of the force equation using reciprocal relations.
[55] H. H. Hu and D. D. Joseph, Numerical simulation of viscoelastic flow past a cylinder, J. Non-Newtonian Fluid Mech. **37**, 347 (1990).
[56] G. H. McKinley, R. C. Armstrong, and R. Brown, The wake instability in viscoelastic flow past confined circular cylinders, Philos. Trans. R. Soc. London, Ser. A **344**, 265 (1993).
[57] M. A. Alves, F. T. Pinho, and P. J. Oliveira, The flow of viscoelastic fluids past a cylinder: Finite-volume high-resolution methods, J. Non-Newtonian Fluid Mech. **97**, 207 (2001).
[58] R. G. Larson, in *The Structure and Rheology of Complex Fluids*, Topics in Chemical Engineering Vol. 86 (Oxford University Press, New York, 1999), p. 108.